PERGAMON

Journal of Structural Geology 25 (2003) 197–208

JOURNAL OF STRUCTURAL GEOLOGY

www.elsevier.com/locate/jsg

Hanging wall fault kinematics and footwall collapse in listric growth fault systems

J. Imber[a,b], C. Childs[a,b,*], P.A.R. Nell[a,c], J.J. Walsh[a,b], D. Hodgetts[d], S. Flint[d]

[a]*Formerly at: Fault Analysis Group, Department of Earth Sciences, 4 Brownlow Street, University of Liverpool, Liverpool L69 3GP, UK*
[b]*Fault Analysis Group, Department of Geology, University College Dublin, Belfield, Dublin 4, Ireland*
[c]*Badley Earth Sciences Ltd., North Beck House, Hundleby, Spilsby, Lincolnshire PE23 5NB, UK*
[d]*Sequence Stratigraphy Group, Department of Earth Sciences, 4 Brownlow Street, University of Liverpool, Liverpool L69 3GP, UK*

Received 8 May 2001; recieved in revised form 14 January 2002; accepted 26 February 2002

Abstract

We describe the structure of a listric growth fault system from SE Asia, using high-resolution, 3-D seismic data. The fault system shows systematic changes in geometry and kinematics that are sympathetic with along-strike changes in the structure of the bounding fault. Where the position of the bounding fault remained fixed, there is an overall landward decrease in the age of the hanging wall growth faults. Along strike, three phases of footwall collapse caused by the active bounding fault stepping back into the footwall block were responsible for the punctuated, stepwise, landward migration of the rollover hinge and associated hanging wall growth faults during extension. The migration of these hanging wall structures is similar to that predicted by simple analogue models with *fixed* detachment surfaces: care should therefore be taken in defining kinematic models in areas where the geometry of the bounding fault is either poorly defined or unknown.

Keywords: Growth fault; Footwall collapse; Rollover; Kinematics

1. Introduction

Listric growth faults are characteristic of thin-skinned, gravity-driven deformation in sequences of poorly lithified sediment (Bally et al., 1981; Roberts and Yielding, 1994). Well documented examples include the Nile Delta (Beach and Trayner, 1991), the Baram Delta (Sandal, 1996) and the US Gulf Coast Basin (Lopez, 1990). In listric growth fault systems, a concave-upwards bounding fault ('basal detachment') is overlain by a thick 'wedge' of pre- and syn-faulting hanging wall sediments (Shelton, 1984; Fig. 1). A characteristic feature of all listric faults is a geometrically-necessary rollover anticline, which develops in the hanging wall above the curved bounding fault surface (e.g. Gibbs, 1984). Complex hanging wall strains are a direct consequence of rollover (e.g. Kerr and White, 1992) and are commonly observed to be accommodated by arrays of planar and/or listric growth faults developed around the crest of the anticline (Gibbs, 1984; Roberts and Yielding, 1994; Fig. 1). We show that in certain circumstances, the rollover hinge (defined as the line marking the basinward limit of pronounced sediment thickening towards the bounding fault) and associated hanging wall growth faults appear to migrate in a landward direction as the hanging wall block is displaced (Fig. 1).

Our understanding of the geometric and kinematic evolution of listric growth fault systems has, in recent years, been significantly improved through the use of scaled, 2-D and 3-D analogue models (e.g. Ellis and McClay, 1988; Vendeville and Cobbold, 1988; McClay et al., 1991; Vendeville, 1991). Typically, these models comprise a deformable hanging wall, composed of unconsolidated sand, clay and/or silicone putty layers, which is extended over a rigid footwall block (Ellis and McClay, 1988). The geometry and position of the bounding fault are determined by the footwall block and therefore remain fixed throughout the model run. Deformation in the hanging wall is controlled by the curvature of the rigid footwall block (McClay et al., 1991; McClay, 1996). Several authors have, however, suggested that footwall collapse—where the bounding fault steps back into the previously undeformed footwall block—could be an important mechanism during the growth of listric fault systems (Gibbs, 1984; Vendeville, 1991). Footwall collapse is difficult to establish unequivocally from natural datasets and is extremely difficult to model experimentally (Roberts

* Corresponding author. Tel.: +353-1-716-2606; fax: +353-1-716-2607.
E-mail address: fault@fag.ucd.ie (C. Childs).

0191-8141/02/$ - see front matter
PII: S0191-8141(02)00034-2

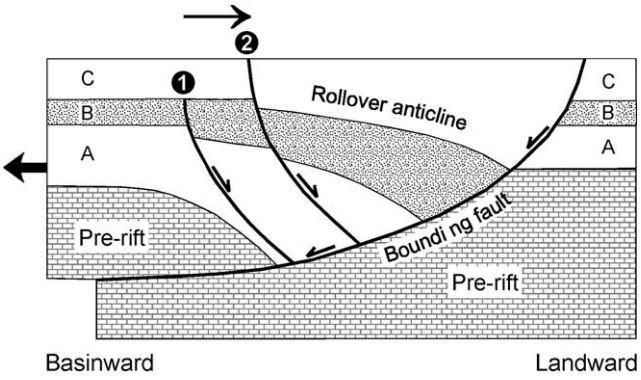

Fig. 1. Cartoon summarising the principal features of listric growth fault systems. Packages of syn-faulting sediments in the hanging wall to the bounding fault (units A, B and C) are deformed by a geometrically-necessary rollover anticline. The rollover anticline is cut by two growth faults (faults 1 and 2) that define the onset of pronounced sediment thickening toward the bounding fault (i.e. the rollover hinge). Across-fault sediment thickness variations show that fault 1 was active during the deposition of unit B and that fault 2 was active throughout the deposition of unit C. Thus, the locus of active hanging wall growth faulting and the rollover hinge appear to have migrated in a landward direction through time (arrow), a feature predicted by 2-D sandbox models of listric growth faults (e.g. McClay, 1990a,b).

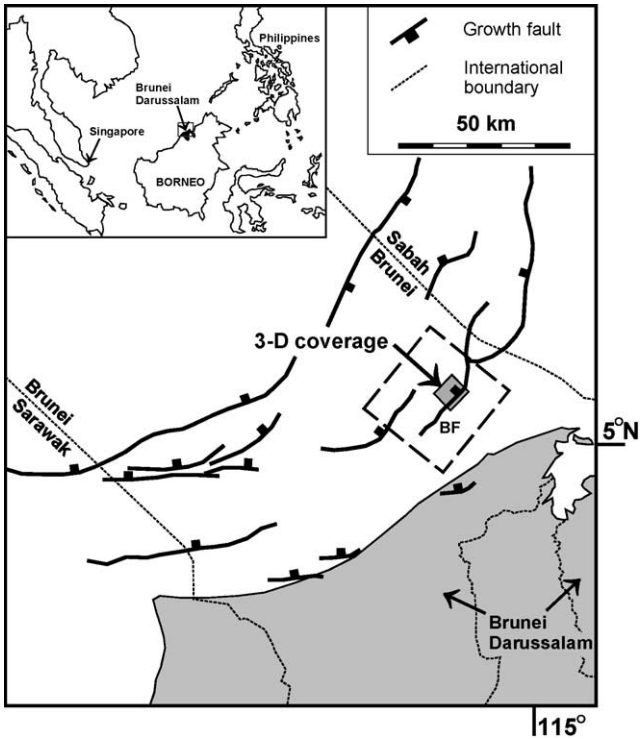

Fig. 2. Map showing the locations and trends of major growth faults, offshore Brunei Darussalam. The 3-D seismic volume (shaded) is located in the hanging wall of a NW-dipping listric growth fault ('bounding fault'). The box (dashed outline) shows the location of Fig. 9a. BF is the bounding fault discussed in the text. Inset is a map of SE Asia showing the location of Brunei Darussalam.

and Yielding, 1994). Consequently, the effects of footwall collapse on the timing and distribution of deformation in the hanging walls to listric growth faults are poorly understood. In this article, we describe the structure of a Late Miocence age listric growth fault developed in a sand/shale, shoreface/tidal estuarine sequence from offshore Brunei Darussalam (Fig. 2), using a high-resolution 3-D acoustic impedance dataset (Hodgetts et al., 2001). Crucially, the dataset provides good definition of both the hanging wall structure and the bounding fault. Along-strike changes in the style of footwall deformation allow us to compare directly the geometry and kinematics of structures developed above a 'fixed' bounding fault with those developed above a zone of repeated footwall collapse (Fig. 3a). We discuss our observations in the light of previously published 2-D analogue models and conclude that footwall collapse is an important, though previously little studied, control on the development of listric growth fault systems.

2. Deformation in the hanging wall of a natural listric growth fault

The 3-D survey volume occupies the uppermost 2 km of a major, NW-dipping growth fault system (Figs. 2 and 3). Estimated vertical displacements (i.e. throws) on the bounding fault vary from ca. 150 m at the top of the mapped hanging wall sequence (Horizon I, Fig. 3b) to ca. 480 m near the base. In the southern part of the survey area, the mapped A to I sequence thickens markedly into the hanging wall rollover (Fig. 4a and b). This observation indicates that the growth fault was active during the deposition of the A to I interval in the southern part of the survey area. 7.5 km to the north, sequence thickening into the hanging wall rollover is clearly observed within the mapped D to I interval (Fig. 4c and d), indicating that the growth fault was active during the deposition of the D to I sequence. Owing to the locally poor quality of the seismic data, it has not been possible to map reflectors corresponding to the older A, B or C horizons into the northern part of the survey area. Nevertheless, the simplest interpretation is that the growth fault was active in both the northern and southern regions throughout A to I times.

A broad, NE–SW trending whaleback anticline (i.e. a pericline) is superimposed upon, and has 'tightened up', the hanging wall rollover anticline associated with the major growth fault. A reflector near the top of the seismically imaged sequence has been correlated from the hanging wall into the footwall of the bounding fault, and shows that the crest of the pericline is at a greater elevation than the footwall block (Fig. 3b). The fold crest is everywhere truncated by the horizontal sea-floor reflector, and a syncline is locally developed in the immediate hanging wall of the bounding fault (Fig. 3b). The syncline is tightest adjacent to the crest of the pericline and the amplitude of the syncline is approximately proportional to that of the anticline: this sympathetic relationship suggests that the syncline and

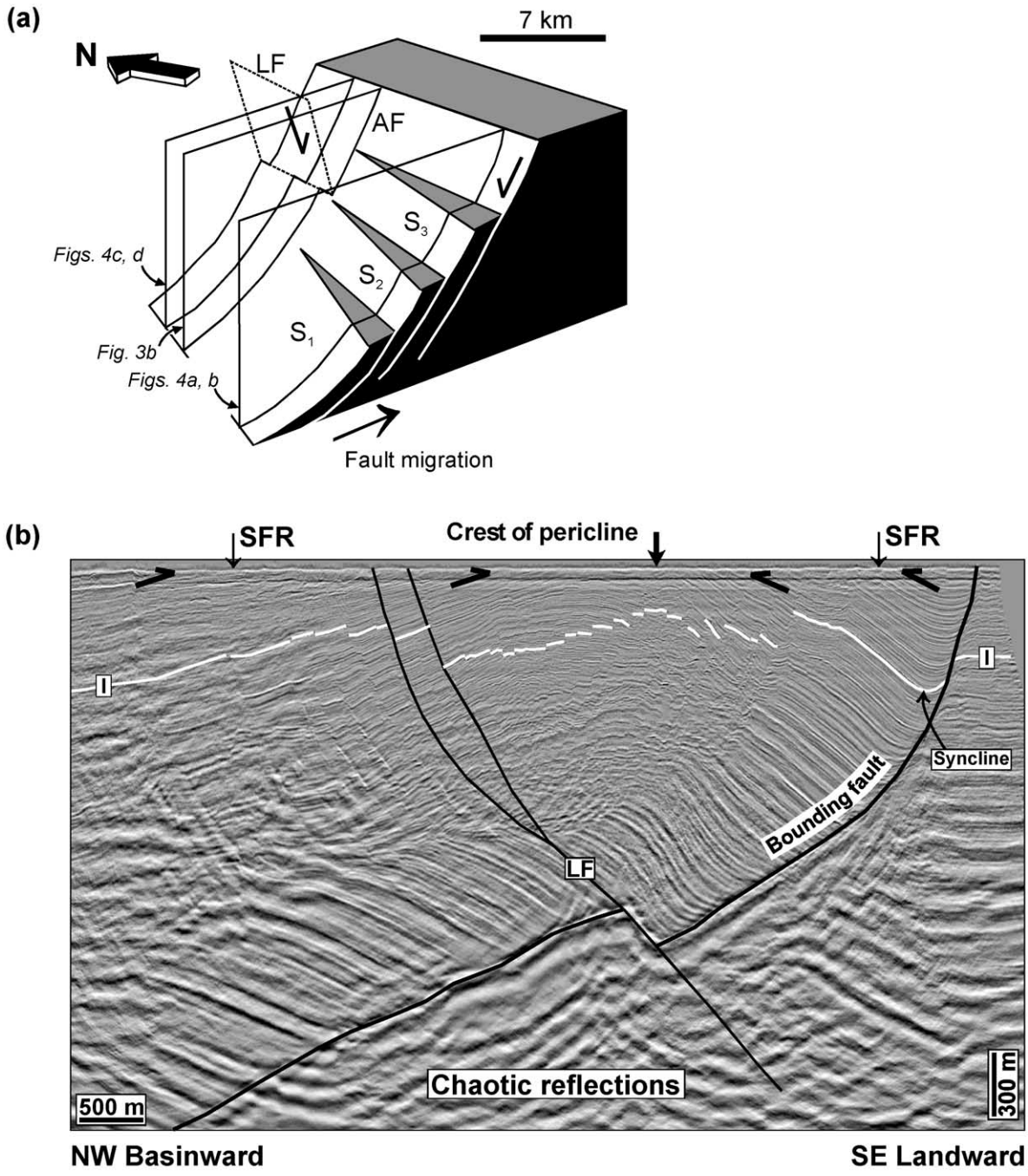

Fig. 3. (a) Cartoon showing the along-strike changes in the structure of the NW-dipping bounding fault together with the locations of the seismic sections in (b) and Fig. 4. S_1, S_2, and S_3 are the landward-stepping fault segments that make up the bounding fault in the southern part of the study area (Fig. 4a). Further north, the bounding fault is a single surface (AF) that is offset across a zone of landward-dipping normal faults (LF = faults 10 and 11 in Fig. 4c). (b) Seismic section through the northern part of the study area showing the listric bounding fault, the hanging wall pericline and associated syncline. The uppermost mapped horizon (I) is structurally higher in the hanging wall than in the footwall of the bounding fault and the crest of the pericline is everywhere truncated (half arrows) by the sea floor reflection (SFR). Note that the bounding fault surface has been offset by late movement on two SE-dipping normal faults (LF)—see text for explanation.

anticline developed at the same time. We attribute folding, erosion (reflector truncation) and uplift of the hanging wall relative to the footwall to a phase of structural inversion following the cessation of active growth faulting (see also Sandal 1996). The crest of the pericline is cut by a network of conjugate normal faults (Fig. 4). These faults are not associated with any across-fault sediment thickness variations and therefore post-date sedimentation in the hanging wall rollover. The conjugate faults are interpreted to have developed in response to crestal collapse of the pericline during and/or following the late-stage structural inversion event.

The western limb of the pericline is cut by arrays of predominantly SE-dipping normal faults i.e. faults that are antithetic to the bounding fault. Pronounced across-fault sediment thickness variations within the mapped A to I interval demonstrate that these normal faults partly accommodated the rollover-related sequence thickening and thus are interpreted to have been active at the same time as extension on the bounding fault (Fig. 4b and d). As we shall show in the following sections, the kinematic evolution of these growth faults provides important insights into the development of the listric fault system as a whole.

2.1. Deformation above a 'fixed' bounding fault

In the northern part of the listric fault system the bounding fault is imaged as a continuous reflection down to ca. 1.8 km depth (Fig. 4c and d). It separates packages of coherent reflectors in the hanging wall from irregular, low frequency seismic events below. Comparison with previous studies conducted in similar structural and sedimentological settings in offshore Brunei Darussalam (Van Rensbergen et al., 1999; Van Rensbergen and Morley, 2000), suggest these 'chaotic' reflections may represent fractured, overpressured shales preserved in the footwall of the major growth fault. This interpretation has not, however, been tested in wells in the study area. The dip of the fault decreases towards the NW, although this trend is locally reversed across a prominent culmination where the bounding fault is offset by a SE-dipping normal fault which splays upwards into two faults labelled 10 and 11 on Fig. 4c (cf. McClay 1990a, fig. 16). The total vertical displacement of the youngest mapped horizons (I and J) across faults 10 and 11 approaches or is equal to the vertical offset of the bounding fault (Figs. 3b and 4c). The absence of significant thickening of the post-I to J interval across faults 10 and 11 indicates that offset of the bounding fault must largely post-date the deposition of the hanging wall sequence. These observations are consistent with offset of the bounding fault having occurred during crestal collapse during late-stage structural inversion. The bounding fault would, therefore, have had a smooth, listric geometry during active growth faulting (cf. Fig. 1). It is apparent, however, from the marked thickening of the G to I interval across fault 10 (Fig. 4d) that this fault also had an earlier growth history that pre-dates offset of the bounding fault surface: the kinematics of the hanging wall growth faults are discussed below.

Growth faults cutting the rollover anticline predominantly dip towards the SE and tip-out within or immediately above, the mapped hanging wall sequence (faults 1–15 on Fig. 4c). Fig. 5a shows the period of activity for individual growth faults within the fault array as determined from across-fault sequence expansion and displacement variations on a number of cross-sections along the strike of the faults (see Childs et al., 1993, 1995 for details). Faults 1 and 2 initiated synchronously with the deposition of the E horizon, whilst activity on fault 3 began at D times, at the latest. Faults 4, 6, 8 and 10 initiated synchronously with, or immediately prior to, the deposition of horizon G, whilst faults 5, 7 and 9 initiated around the time the H horizon was deposited (Fig. 5a). Activity on faults 11 to 15 began after the deposition of horizon I. There is considerable overlap between the periods of activity on individual faults and, apart from faults 5–7 and 15, they display an overall increase in upper tip-line elevation towards the SE (Figs. 4c and 5a). Thus, our observations show that faults tend to young in a landward direction and that the width of the zone of active faulting varied in time from ca. 0.8 to 2.6 km. Possible controls on the apparent 'out-of-sequence' development of faults 3, 5–7 and 15 (Fig. 5a) are discussed in Section 3.

The rollover hinge (i.e. the line marking the basinward limit of sequence expansion in the hanging wall of the bounding fault) was, at any time during the deposition of the seismically imaged sequence, marked by one or other of the SE-dipping growth faults. The rollover hinge was defined by faults 3 and 1 during the deposition of the D to E and E to H sequences, respectively (Figs. 4d and 5a). The hinge was defined by fault 2 during the deposition of the lowermost H to I interval, and by fault 3 when the upper part of this sequence was deposited (Figs. 4d and 5a). In the youngest I to J interval, the rollover hinge was initially marked by fault 4, then by fault 10 during deposition of the upper part of this sequence (Figs. 4d and 5a). Thus, apart from an early, basinward shift associated with 'out-of-sequence' activity on fault 3 (Fig. 5a), the rollover hinge shows evidence for progressive, southeastward (i.e. landward) migration during extension.

Fig. 4. (a) Seismic section through the southern part of the study area showing the segmented bounding fault (comprising the present-day fault surface, AF, and three older splay faults, S_1 to S_3) and associated hanging wall anticline. Horizons D to I have been mapped across the entire study area; horizons A to C have been mapped only within the southern part of the study area. The anticline is cut by two distinct sets of normal faults: growth faults which were active during the deposition of the mapped hanging wall sequence (black), and younger, conjugate faults (grey) that post-date the deposition of the imaged sequence. SFR is the sea floor reflector. (b) Seismic section in (a) highlighting five packages of syn-faulting sediments (A to B, B to C, C to F, F to H and H to I). The arrows (H_{A-B} etc.) mark the basinward limit of sequence thickening (i.e. the rollover hinge) for each package of sediments. Collapse-related conjugate faults not shown. (c) Seismic section through the northern part of the study area showing the listric bounding fault (AF) and associated rollover anticline. The anticline is cut by predominantly SE-dipping growth faults (black) and younger, conjugate faults which post-date the deposition of the seismically-imaged sequence (grey). The bounding fault surface has been offset by later (post-depositional) movement along faults 10 and 11. (d) Seismic section in (c) highlighting four packages of syn-faulting sediments (D to E, E to H, H to I and I to J). The arrows (H_{D-E} etc.) show the position of the rollover hinge during the deposition of each of the mapped sequences. Collapse-related conjugate faults not shown. Note that the fault numbering in (a) is independent of that in (c) and the numbers do not imply along-strike fault correlation.

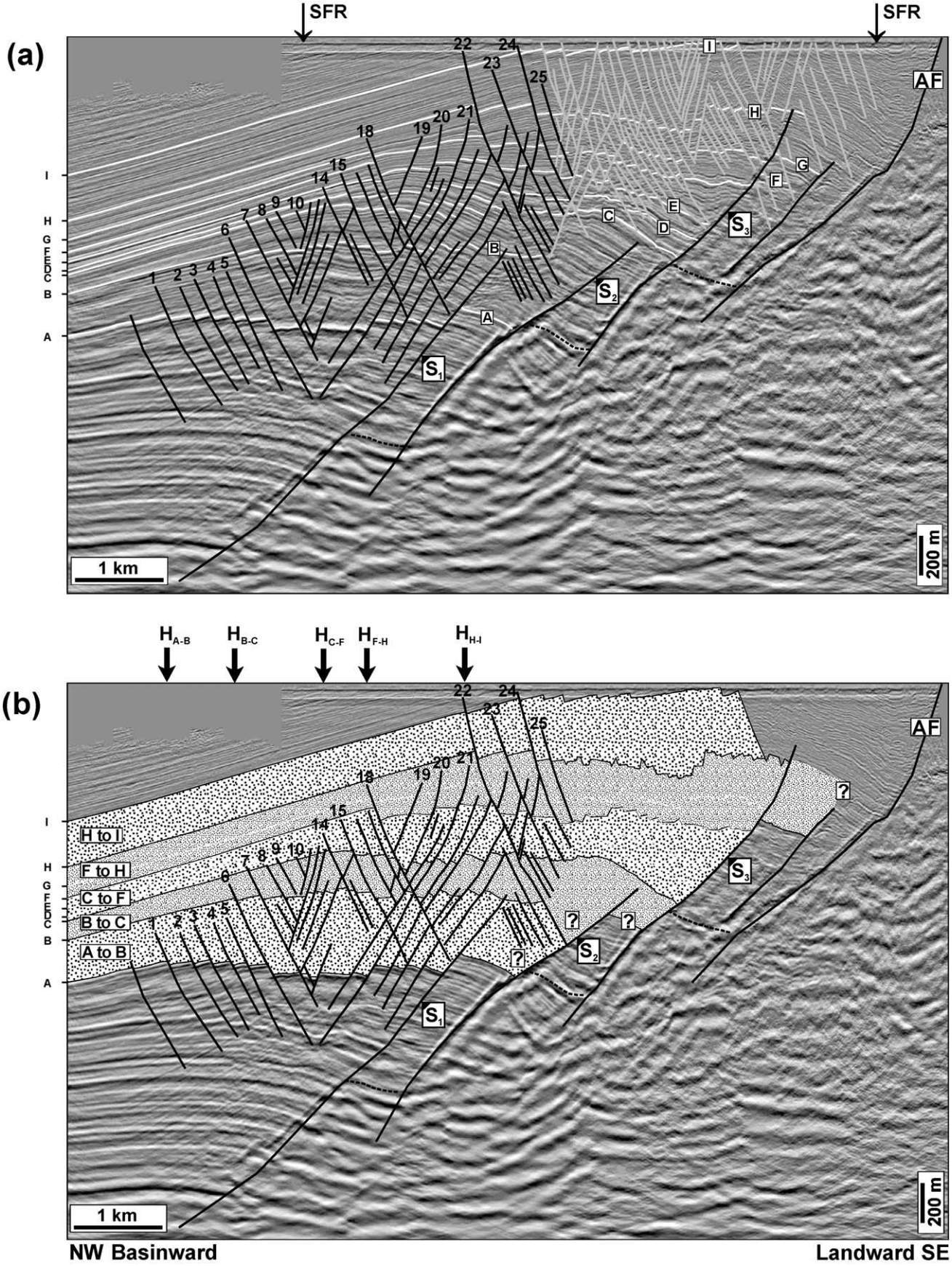
(a)
SFR
SFR
AF
I
H
G
F
E
D
C
B
A
1 2 3 4 5 6 7 8 9 10 14 15 18 19 20 21 22 23 24 25
S1
S2
S3
1 km
200 m
(b)
HA-B
HB-C
HC-F
HF-H
HH-I
H to I
F to H
C to F
B to C
A to B
?
NW Basinward
Landward SE

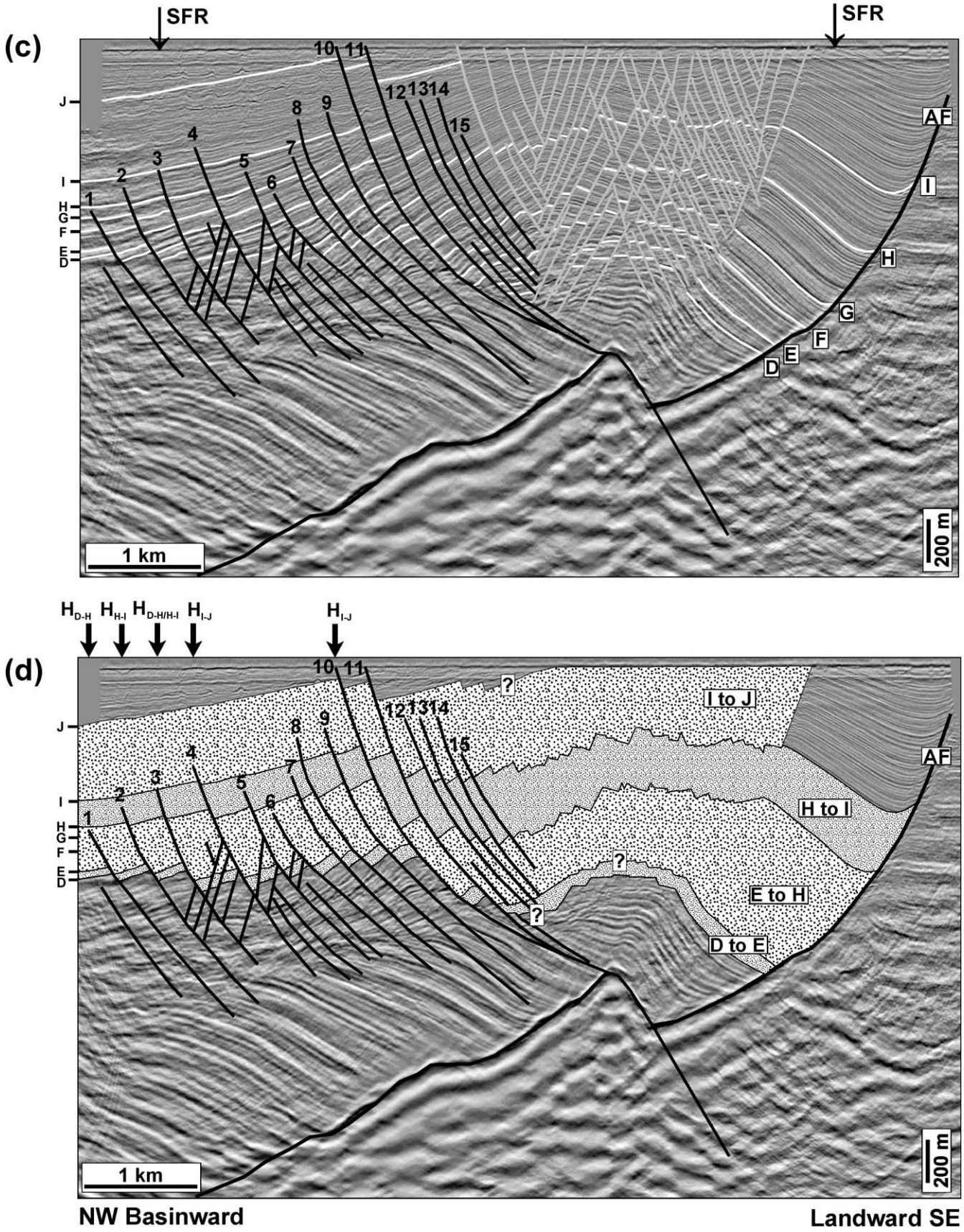

Fig. 4. (*continued*)

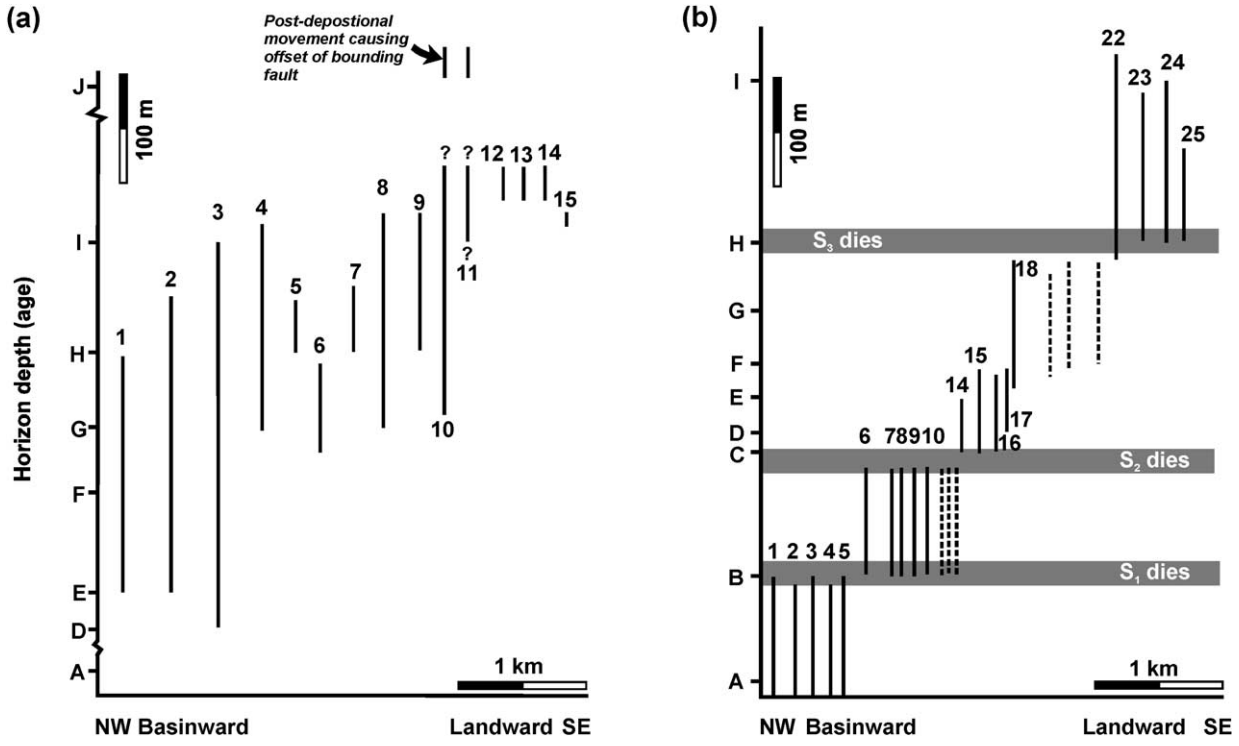

Fig. 5. Fault activity diagrams for hanging wall growth faults in (a) the northern and (b) southern parts of the fault system. Bold vertical lines show the period of activity on individual SE-dipping hanging wall growth faults as determined from across-fault sediment thickness variations and the upper tip-line elevations (see Childs et al., 1993). The numbers correspond to the faults in Fig. 4c. In (b), the dashed vertical lines represent the periods of activity on NW-dipping growth faults (Fig. 4a). Grey horizontal lines show the times at which different segments of the bounding fault (Fig. 4a) became inactive.

2.2. Deformation above a 'backstepping' bounding fault

In the southern part of the survey volume, the bounding fault is imaged as an array of NW-dipping reflectors—comprising the present-day bounding fault surface (AF in Fig. 4a) and three older 'splay' faults (S_1 to S_3 in Fig. 4a) that separate packages of coherent reflectors in their hanging walls from irregular, low frequency seismic events below (see Section 2.1). The F to G interval thickens by ca. 30% across the easternmost splay fault (S_3) which tips-out immediately above horizon H (Fig. 4a). These observations show that the S_3 splay was active during the deposition of the F to H interval and that the fault became inactive shortly after the deposition of horizon H. The upper tip-line elevation of the S_2 splay suggests that it ceased moving just before horizon C was deposited (Fig. 4a). The locally poor quality of the data precludes more precise dating of activity on the S_2 fault. The westernmost splay (S_1) tips out just above horizon B. Although the complex structure and highly rhythmic nature of the reflectors preclude confident correlation of the A horizon into the footwall of S_1, our preferred interpretation indicates a ca. 35% thickening of the A to B sequence across S_1 (Fig. 4a and b). These observations imply that S_1 was active during the deposition of the A to B interval and that the fault became inactive shortly after the deposition of horizon B. The data show unequivocally that the splay faults became inactive at successively later times towards the SE, and are also consistent with the age of fault initiation decreasing in a landward direction. Thus, the splay faults appear to young towards the present day bounding fault. Such age relationships are consistent with the SE-stepping splay faults having formed by footwall collapse along the main bounding fault (Fig. 6). We envisage the death of each older (i.e. more westerly) fault to have been caused by the active fault surface stepping SE into the footwall (Fig. 6a). The resulting splay fault was subsequently buried and preserved by younger sediments deposited conformably in the hanging wall of the newly active bounding fault (Fig. 6b); this process generates structures that are equivalent to the intrabasinal highs of Anders and Schlische (1994). An important corollary of our model is that at any one time, the *active* strand of the bounding fault would have had a smooth profile, not a stepped geometry as implied by the present day trace of the bounding fault surface. We shall now describe the distribution and timing of hanging wall deformation above this zone of repeated footwall collapse.

Growth faults preserved in the hanging wall of the main bounding fault predominantly dip towards the SE, and their upper tip-line elevations generally increase from NW to SE across the study area (faults 1–25 on Fig. 4a). Fig. 5b shows the period of activity for individual growth faults within the hanging wall fault array on a plot of horizon depth (as a proxy for age) versus distance along the seismic section. The growth faults define four spatially and temporally

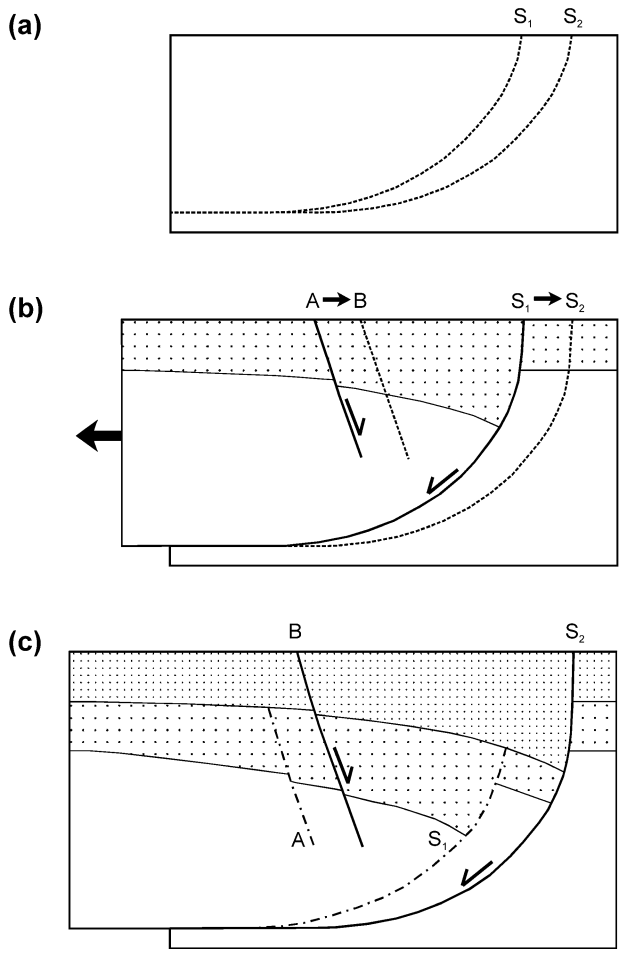

Fig. 6. Model of hanging wall growth fault migration in response to footwall collapse along the bounding fault. Bold solid lines are active faults, dashed lines are faults that have not yet formed and faults that are inactive are shown with a dot-dash ornament. (a) Undeformed 'template' showing the future positions of the bounding fault. (b) The bounding fault (S_1) steps back into the footwall causing the hanging wall growth faults to step in the same direction. (c) The original position of the bounding fault is marked by a 'dead' splay (S_1) which is carried passively in the hanging wall of the active bounding fault surface (S_2). Newly deposited sediments (fine stipple) blanket the splay fault and conformably overlie the older sediments (coarse stipple) deposited in the footwall of S_1.

distinct groups, comprising: faults 1–5, faults 6–13, faults 14–21 and faults 22–25 (Fig. 5b). The zone of active growth faulting therefore varied from ca. 0.7 to 1.1 km wide at different times during extension. This variation is significantly less than that observed above the 'fixed' bounding fault (Section 2.1). The period of activity on individual growth faults overlapped, to a greater or lesser extent, with the period of activity on neighbouring faults within the *same* group. Each individual group of faults is older than all other groups to the SE, and there is no spatial or temporal overlap between neighbouring groups of faults. Thus, there is very clear evidence for systematic, stepwise SE-migration of the hanging wall growth faults during extension.

Sediment thickness variations show that the rollover hinge was defined by one or other of the SE-dipping growth faults during the deposition of the mapped A to I sequence. Faults 1, 6, 14, 18 and 22 marked the basinward limit of sequence expansion during the deposition of the A to B, B to C, C to F, F to H and H to I intervals, respectively (Fig. 4b). Thus, in the southern part of the study area there is clear evidence for systematic, landward migration of the rollover hinge through time.

The SE migration of the rollover hinge and associated hanging wall growth faults is temporally related to the death of individual seismically imaged splay faults (S_1, S_2 and S_3; Fig. 4a) on the underlying bounding fault. The death of hanging wall growth faults 1–5 and the initiation of faults 6–13 occurred at the same time as the death of the S_1 splay. Similarly, the death of faults 6–13 and the initiation of faults 14–17 correspond to the time when the S_2 splay became inactive, and the initiation of faults 22–25 and the cessation of activity on faults 18–21 occurred when the S_3 splay died (Fig. 5b). The rollover hinge and associated hanging wall growth faults, therefore, migrated in sympathy with the SE-stepping bounding fault (Fig. 6). Thus, repeated footwall collapse appears to have been the main control on punctuated hanging wall deformation in the southern part of the 3-D study area. In the following discussion, we compare the natural fault system with the structures predicted by a simple, 2-D sandbox model and then consider possible causes of footwall collapse.

3. Discussion

3.1. Comparison with a 2-D analogue model

In sandbox model E44 (McClay, 1990b), a fixed listric bounding fault passes down into a gently 'basinward'-dipping detachment. The detachment is overlain by a deformable hanging wall and sediment (unconsolidated sand) is added to the hanging wall such that the sedimentation rate keeps pace with the fault displacement rate throughout the experiment (McClay, 1996; Fig. 7). The boundary conditions imposed by this model geometry are similar to the boundary conditions which we infer to have been operative during deformation above the 'fixed' bounding fault in the northern part of the seismic study area (Fig. 4c and d). Within the modelled hanging wall rollover, the basinward limits of sediment thickening in the A–E growth intervals are narrow zones defined by 'landward'-dipping (i.e. antithetic) growth faults 1, 2, 4, 7 and 8, respectively (Fig. 7). Across-fault sediment thickness variations show that (a) the age of these antithetic faults decreases in a 'landward' direction, and (b) there is considerable overlap between the periods of activity on individual hanging wall growth faults (Figs. 7 and 8). Thus, the model predicts that the rollover hinge and associated hanging wall growth faults should migrate progressively landward. This fault pattern arises because the hanging wall growth faults nucleate in the sediment volume above the point at which the

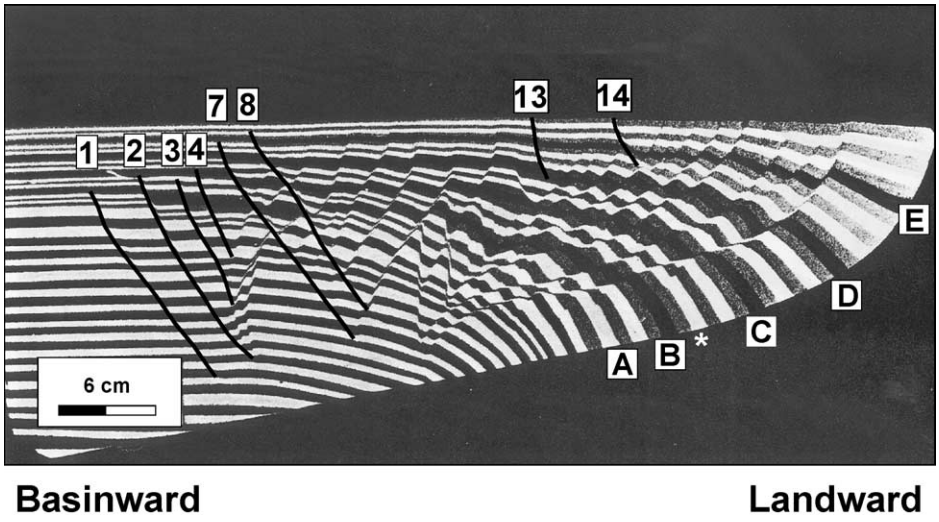

Fig. 7. McClay's (1990b) 2-D sandbox experiment E44 at 100% model extension. Regularly spaced markers are pre-rift sediments, alternating wide/narrow markers are syn-rift sediments (labelled A to E). The point at which the curved bounding fault flattens out into a gently 'basinward'-dipping detachment is marked with a star (*).

detachment surface flattens out (Fig. 7), causing an apparent migration of the active growth faults towards the bounding fault as the hanging wall block is displaced away from the footwall ('listric fault mechanism'; McClay, 1990a; McClay et al., 1991).

The fault pattern observed in the northern part of the seismic volume—i.e. an overall decrease in the age of faulting in a landward direction, and significant overlap in the periods of activity on individual growth faults—is broadly consistent with the fault pattern predicted by 2-D sandbox models, implying that a listric fault mechanism could have been an important control on deformation in the hanging wall of the 'fixed' bounding fault (Figs. 5a and 8). Faults 5–7 and 15 do not, however, fit this pattern because they became inactive before neighbouring faults in more basinward locations, whilst fault 3 was active before faults 1 and 2 (Fig. 5a). This 'out-of-sequence' faulting is most simply explained by 3-D (i.e. out of plane) effects—such as along-strike changes in the geometry of the bounding fault and/or segment linkage across relay zones (e.g. Childs et al., 1993; see below)—that cannot be captured by 2-D sandbox models. In the southern part of the seismic volume, a listric fault mechanism could explain the death of faults 14–17 and the onset of activity along faults 18–21 (Figs. 4a and 5b), but it is clear that footwall collapse must have been the first-order control on the punctuated fault migration in the hanging wall rollover.

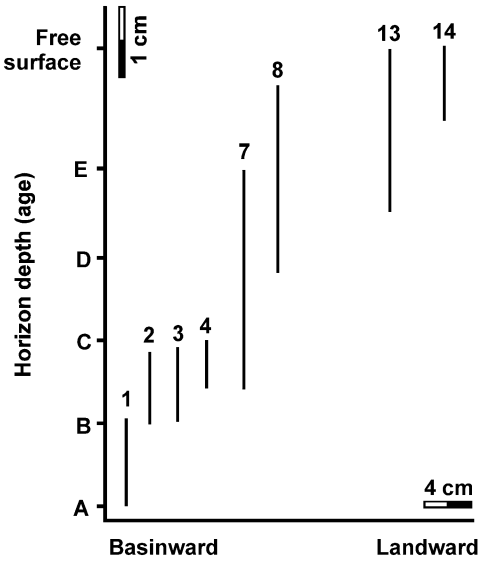

Fig. 8. Fault activity diagram for 'landward' dipping hanging wall growth faults in McClay's (1990b) sandbox experiment E44. The bold vertical lines show the period of activity on individual growth faults as determined from across-fault sequence thickening. The numbers correspond to the faults shown in Fig. 7.

3.2. Possible causes of footwall collapse

Based on data from the northern North Sea, a largely sediment-starved basin, previous authors have suggested that footwall collapse may be triggered by gravity-induced slumping at fault scarps during unloading and relative uplift of overpressured rocks in the footwalls of normal faults (Gibbs, 1984; Berger and Roberts, 1999; Hesthammer and Fossen, 1999; McLeod and Underhill, 1999). These slump-related faults, which are characterised by listric profiles and curvilinear map traces (Hesthammer and Fossen, 1999), are commonly observed where the hanging wall basin is underfilled (e.g. McLeod and Underhill, 1999). On the scale of the present study area, the bounding fault is characterised by a straight map trace (Fig. 2) and there is no seismic evidence for the development of major fault scarps. Independent burial history analyses show that sedimentation rates during the period of active growth faulting were extremely high (up

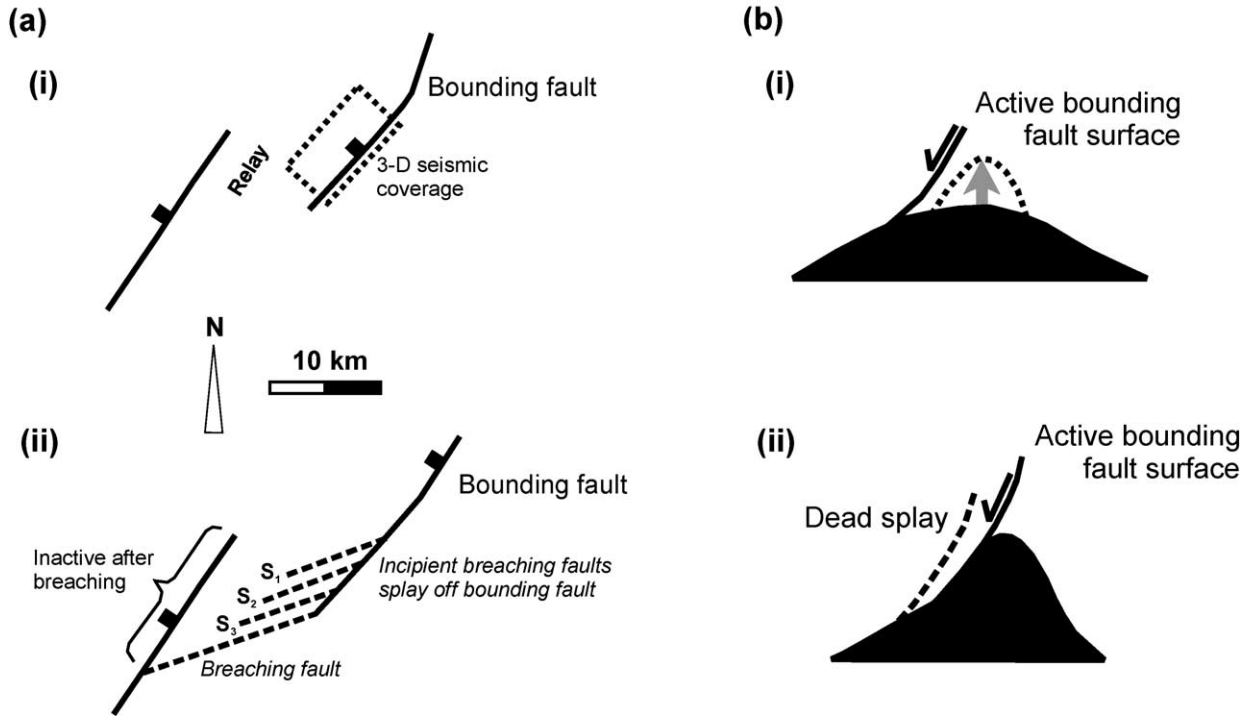

Fig. 9. Cartoons showing possible causes of footwall collapse. (a) Model for footwall collapse by relay breaching. (i) Map showing the study area in relation to two regionally important growth faults (Fig. 2b). (ii) The splay faults (S_1 to S_3; Fig. 4a) are interpreted as incipient breaching faults that cut back across the relay zone. The breaching fault is equivalent to the present day bounding fault surface (AF in Fig. 4a) (b) Model for footwall collapse above a rising shale diapir. (i) A shale 'roller' develops in the footwall of the active fault during the early stages of diapirism. (ii) As the diapir rises, it narrows. In order to maintain strain compatibility, the active surface of the growth fault 'steps-back' into the footwall, leaving a dead splay (dashed) preserved in the hanging wall.

to ca. 1000 m/my; Sandal, 1996), and we have found no stratigraphic indications (e.g. incised valleys and/or widespread unconformities) for underfilling of the basin (see Hodgetts et al., 2001). These observations suggest that gravitationally-induced slumping of prominent footwall scarps was *not* the main cause of footwall collapse in the SE Asian study area. We outline two possible mechanisms which are consistent with the currently available structural and stratigraphic data: (a) fault 'backstepping' by segment linkage across a large relay zone, and (b) footwall collapse above a rising shale diapir.

3.2.1. Segment linkage across a relay zone

Proprietary regional seismic lines show that the study area lies between two en-échelon, right-stepping, NW-dipping growth faults ca. 12 km apart. The southeastern growth fault forms the bounding fault to the 3-D seismic survey area (Figs. 2 and 9a). Across-fault sediment thickness variations indicate that the periods of activity on both faults overlapped, but that activity on the hanging wall fault ceased *before* the footwall fault. Such geometric and age relationships, though not conclusive, are consistent with the study area being located within a large relay which, prior to failure by probable footwall breaching (e.g. Peacock and Sanderson, 1991; Childs et al., 1993; Walsh et al., 1999), transferred displacement between the two NW-dipping growth faults (Fig. 9a). We suggest that the 'backstepping' events observed within the 3-D study area could represent a series of internal faults cutting back from NE to SW across the relay zone. The relative ages and orientations of the intra-relay faults in this model (Fig. 9a) are consistent with both the relative ages of the seismically imaged splay faults, and the geometries expected for relay breaching by footwall failure (e.g. Childs et al., 1993, figs. 2 and 3).

3.2.2. Footwall collapse above a shale diapir

In areas of rapid sedimentation and growth faulting, chaotic seismic facies such as those observed in the footwall of the main bounding fault (Fig. 4) are commonly interpreted as masses of fractured, overpressured clay or shale (e.g. Doust and Omatsola, 1990; Sandal, 1996; Van Rensbergen et al., 1999; Van Rensbergen and Morley, 2000). It has been proposed that such clay/shale bodies are highly mobile and may form diapirs in the footwalls of regional-scale growth faults (Doust and Omatsola, 1990; Van Rensbergen et al., 1999; cf. Van Rensbergen and Morley, 2000). Assuming the behaviour of the mobile shale is akin to that of salt (Lopez, 1990, but see discussion in Morley and Guerin, 1996), the early stages of shale diapirism are likely to be characterised by the development of a low amplitude, long wavelength 'roller' (e.g. Szatmari et al., 1996, fig. 6) which narrows progressively as the diapir rises (e.g. Allen and Allen, 1990, fig. 10.63). This shape change could be responsible for the bounding fault

backstepping towards the rising diapir (Fig. 8b; cf. Morley and Guerin, 1996, figs. 10 and 14). Footwall collapse in the southern part of the seismic study area could, therefore, have been triggered by, and may 'track' the gradual rise and narrowing of a large shale diapir in the footwall of the main bounding fault. Accentuated diapirism in the southern part of the fault system may be linked to the existence of the large relay zone in the area (Fig. 2).

3.2.3. Kinematics of hanging wall deformation

The currently available data do not allow us to determine unequivocally which, if either, of these mechanisms for footwall collapse is correct. Our study shows, however, that systematic variations in the style of hanging wall deformation relate directly to along-strike variations in the structure and geometry of the bounding fault. These results have important implications for defining structural/kinematic models in areas of listric growth faulting, especially where the bounding fault/basal detachment is either poorly imaged or poorly exposed. In particular, the spatial and temporal distribution of the hanging wall growth faults must be carefully constrained in order to distinguish between systems characterised by a 'fixed' footwall and systems characterised by footwall collapse. An important corollary of our study is that extreme caution should be exercised when using techniques for deriving the shape of the underlying detachment fault based on hanging wall bed/reflector geometries (e.g. Verrall, 1981; White and Yielding, 1991; Kerr and White, 1992)—assumptions of a fixed, listric fault geometry may not always be valid.

4. Conclusions

- Along-strike variations in the style and distribution of hanging wall deformation in listric growth fault systems are primarily controlled by the behaviour of the underlying bounding fault.
- Deformation above a 'fixed' bounding fault is characterised by significant overlap in the periods of activity of individual hanging wall growth faults and there is a tendency for growth faults in more landward locations to be younger than faults in more basinward locations. Curvature of the bounding fault is likely to be the main control on deformation in the hanging wall rollover.
- Deformation above a zone of repeated footwall collapse is characterised by punctuated migration in the locus of active growth faulting and sediment thickening. Footwall collapse and 'backstepping' of the bounding fault are the first-order controls on deformation in the hanging wall rollover.
- The spatial and temporal distribution of hanging wall growth faults may allow discrimination between deformation above a 'fixed' bounding fault from deformation above a zone of repeated footwall collapse. However, care should be taken when defining structural/kinematic models in regions where the geometry of the bounding fault/basal detachment is poorly constrained.
- The available data indicate that footwall collapse in the study area may have been caused by either segment linkage in a large (regional-scale) relay zone, or in response to the rise of a mobile shale diapir in the footwall to the main bounding fault.

Acknowledgements

This work arose from two studies funded by the Brunei Shell Petroleum Company Sendirian Berhad (BSP) and conducted at the University of Liverpool during 1997–1999. We thank BSP and the Petroleum Unit, Brunei Darussalam for permission to publish this article. W. Taylor and S. Janecke provided constructive reviews that improved the clarity of the manuscript.

References

Allen, P.A., Allen, J.R., 1990. Basin Analysis. Blackwell Science Ltd, Oxford, UK, 451pp.

Anders, M.H., Schlische, R.W., 1994. Overlapping faults, intrabasin highs, and the growth of normal faults. Journal of Geology 102, 165–180.

Bally, A.W., Bernoulli, D., Davis, G.A., Montadert, L., 1981. Listric normal faults. In: Oceanologica Acta: Proceedings of the 26th International Geological Congress, Geology of Continental Margins Symposium, Paris, pp. 87–101.

Beach, A., Trayner, P., 1991. The geometry of normal faults in a sector of the offshore Nile Delta, Egypt. In: Roberts, A.M., Yielding, G., Freeman, B. (Eds.), The Geometry of Normal Faults. Geological Society Special Publication 56, pp. 173–182.

Berger, M., Roberts, A.M., 1999. The Zeta Structure: a footwall degradation complex formed by gravity sliding on the western margin of the Tampen Spur, Northern North Sea. In: Fleet, A.J., Boldy, S.A.R. (Eds.), Petroleum Geology of Northwest Europe. Proceedings of the 5th Conference, pp. 107–116.

Childs, C., Easton, S.J., Vendeville, B.C., Jackson, M.P.A., Lin, S.T., Walsh, J.J., Watterson, J., 1993. Kinematic analysis of faults in a physical model of growth faulting above a viscous salt analogue. Tectonophysics 228, 313–329.

Childs, C., Watterson, J., Walsh, J.J., 1995. Fault overlap zones within developing normal fault systems. Journal of the Geological Society 152, 535–549.

Doust, H., Omatsola, E., 1990. Niger Delta. In: Edwards, J.D., Santogrossi, P.A. (Eds.), Divergent/Passive Margin Basins. AAPG, Tulsa. AAPG Memoir 48, pp. 201–238.

Ellis, P.G., McClay, K.R., 1988. Listric extensional fault systems—results of analogue model experiments. Basin Research 1, 55–70.

Gibbs, A.D., 1984. Structural evolution of extensional basin margins. Journal of the Geological Society 141, 609–620.

Hesthammer, J., Fossen, H., 1999. Evolution and geometries of gravitational collapse structures with examples from the Statfjord Field, northern North Sea. Marine and Petroleum Geology 16, 259–281.

Hodgetts, D., Imber, J., Childs, C., Flint, S., Howell, J., Kavanagh, J., Nell, P., Walsh, J., 2001. Sequence stratigraphic responses to shoreline-perpendicular growth faulting in shallow marine reservoirs of the Champion field, offshore Brunei Darussalam, South China Sea. AAPG Bulletin 85, 433–457.

Kerr, H.G., White, N., 1992. Laboratory testing of an automatic method for

determining normal fault geometry at depth. Journal of Structural Geology 14, 873–885.

Lopez, J.E., 1990. Structural styles of growth faults in the U.S. Gulf Coast Basin. In: Brooks, J. (Ed.), Classic Petroleum Provinces. Geological Society Special Publication 50, pp. 203–219.

McClay, K.R., 1990a. Physical models of structural styles during extension. In: Tankard, A.J., Balkwill, H.R. (Eds.), Extensional Tectonics and Stratigraphy of the North Atlantic Margins. AAPG, Tulsa. AAPG Memoir 46, pp. 95–110.

McClay, K.R., 1990b. Extensional fault systems in sedimentary basins: a review of analogue model studies. Marine and Petroleum Geology 7, 206–233.

McClay, K.R., 1996. Recent advances in analogue modelling: uses in section interpretation and validation. In: Buchanan, P.G., Nieuwland, D.A. (Eds.), Modern Developments in Structural Interpretation, Validation and Modelling. Geological Society Special Publication 99, pp. 201–225.

McClay, K.R., Waltham, D.A., Scott, A.D., Abousetta, A., 1991. Physical and seismic modeling of listric normal fault geometries. In: Roberts, A.M., Yielding, G., Freeman, B. (Eds.), The Geometry of Normal Faults. Geological Society Special Publication 56, pp. 231–239.

McLeod, A.E., Underhill, J.R., 1999. Processes and products of footwall degradation, northern Brent Field, Northern North Sea. In: Fleet, A.J., Boldy, S.A.R. (Eds.), Petroleum Geology of Northwest Europe. Proceedings of the 5th Conference, pp. 91–106.

Morley, C.K., Guerin, G., 1996. Comparison of gravity-driven deformation styles and behavior associated with mobile shales and salt. Tectonics 15, 1154–1170.

Peacock, D.C.P., Sanderson, D.J., 1991. Displacements, segment linkage and relay ramps in normal fault zones. Journal of Structural Geology 13, 721–734.

Roberts, A., Yielding, G., 1994. Continental extensional tectonics. In: Hancock, P.L. (Ed.). Continental Deformation. Pergamon Press, Oxford, pp. 223–250.

Sandal, S.T. (Ed.), 1996. Geology and hydrocarbon resources of Negara Brunei Darussalam. Brunei Shell Petroleum Company Sendirian Berhad and Brunei Museum, Bandar Seri Begawan, Brunei Darussalam. 243pp.

Shelton, J.W., 1984. Listric normal faults: an illustrated summary. AAPG Bulletin 68, 801–815.

Szatmari, P., Guerra, M.C.M., Pequeno, M.A., 1996. Genesis of large counter-regional normal fault by flow of Cretaceous salt in the South Atlantic Santos Basin, Brazil. In: Alsop, G.I., Blundell, D.J., Davison, I. (Eds.), Salt Tectonics. Geological Society Special Publication 100, pp. 259–264.

Van Rensbergen, P., Morley, C.K., 2000. 3D Seismic study of a shale expulsion syncline at the base of the Champion delta, offshore Brunei and its implications for the early structural evolution of large delta systems. Marine and Petroleum Geology 17, 861–872.

Van Rensbergen, P., Morley, C.K., Ang, D.W., Hoan, T.Q., Lam, N.T., 1999. Structural evolution of shale diapirs from reactive rise to mud volcanism: 3D seismic data from the Baram delta, offshore Brunei Darussalam. Journal of the Geological Society 156, 633–650.

Vendeville, B., 1991. Mechanisms generating normal fault curvature: a review illustrated by physical models. In: Roberts, A.M., Yielding, G., Freeman, B. (Eds.), The Geometry of Normal Faults. Geological Society Special Publication 56, pp. 241–249.

Vendeville, B., Cobbold, P.R., 1988. How normal faulting and sedimentation interact to produce listric fault profiles and stratigraphic wedges. Journal of Structural Geology 10, 649–659.

Verrall, P., 1981. Structural interpretation with applications to North Sea problems. Course Notes No. 3, JAPEC (UK).

Walsh, J.J., Watterson, J., Bailey, W.R., Childs, C., 1999. Fault relays, bends and branch-lines. Journal of Structural Geology 21, 1019–1026.

White, N., Yielding, G., 1991. Calculating normal fault geometries at depth: theory and examples. In: Roberts, A.M., Yielding, G., Freeman, B. (Eds.), The Geometry of Normal Faults. Geological Society Special Publication 56, pp. 251–260.